Journal of Catalysis 262 (2009) 73–82

Contents lists available at ScienceDirect

Journal of Catalysis

www.elsevier.com/locate/jcat

In situ preparation of Ni–Cu/TiO_2 bimetallic catalysts

P. Li [a,1], J. Liu [b], N. Nag [c], P.A. Crozier [d,*]

[a] Center for Solid State Science, Arizona State University, Tempe, AZ 85287-1704, United States
[b] Center for Nanoscience, Department of Physics & Astronomy and Department of Chemistry and Biochemistry, University of Missouri-St. Louis, One University Boulevard, St. Louis, MO 63121, USA
[c] BASF Catalysts LLC., 23800 Mercantile Road, Beachwood, OH 44122, USA
[d] School of Materials, Arizona State University, Tempe, AZ 85287-8706, USA

ARTICLE INFO

Article history:
Received 1 July 2008
Revised 27 November 2008
Accepted 1 December 2008
Available online 14 January 2009

Keywords:
Bimetallic catalyst
Incipient wetness
Precursor
Nanoparticles
Nickel–copper
Titania
Preparation
HREM
EELS
Environmental TEM

ABSTRACT

A nanoscale investigation was performed on the initial stages of the formation of nanoparticles during the preparation of NiCu/TiO_2 bimetallic catalysts by incipient wetness impregnation. The evolution of the structure and chemistry of individual nanoparticles was followed in the reaction cell of an environmental transmission electron microscope. During reduction in hydrogen at 300 °C, nuclei quickly formed and grew mainly via Ostwald ripening or short-range particle–particle coalescence. The presence of Cu greatly enhanced the reducibility of the Ni species and about 85% of the particles were metallic. Most of the particles were uniform in composition but approximately 15% of the particles showed Ni enrichment on the surface. The surface enrichment of Ni was attributed to differential diffusion processes and demonstrated that, for the reduction temperature used for this experiment, the structure of the bimetallic particles was controlled by kinetics rather than by thermodynamics.

1. Introduction

Ni-based bimetallic catalysts containing Cu exhibit significantly different catalytic activity and selectivity compared to Ni monometallic catalysts [1–5]. For example, the addition of Cu to Ni enhances the water–gas shift activity in the presence of CO_2 [6], and catalytic activity for ethylene hydrogenation [3,4]. In carbon dioxide hydrogenation, the addition of Cu favors CO formation [5]. The addition of Cu to Ni/Al_2O_3 also increases the selectivity to 1-butene [1]. It was also reported that adding a small amount of Cu to Ni dramatically enhanced the generation of carbon fibers from decomposition of hydrocarbons [7]. Changes in the catalytic properties induced by adding Cu to Ni can be caused by changes in the electronic properties of the homogeneous alloy particle, by the formation of active surface structures, by preferential segregation of one metal to the surface or by a combination of all these effects [6,8–10].

The catalytic properties of bimetallic nanoparticles are directly related to their structure and composition which may be controlled by processes taking place during catalyst preparation. For example, even though Cu has a lower surface free energy than Ni and should, based on thermodynamics, preferentially occupy surface sites [11], core–shell structures with Ni surface enrichment [9] or Cu surface enrichment [10] have been prepared. This indicates that the kinetics associated with the catalyst preparation processes can play a major role in determining the final structure of the bimetallic particles. Classical impregnation techniques have been remarkably successful at synthesizing a wide variety of supported metal catalysts. In the present work, we report on the dynamic processes taking place during the preparation of Ni–Cu bimetallic nanoparticles using the incipient wetness impregnation approach.

Processes involving adsorption, dissociation, diffusion, nucleation, particle growth and phase transformations take place during the preparation of a heterogeneous catalyst. In bimetallic systems, the interaction of the metal species with each other as well as with the support further complicates the process. There is wide recognition of the importance of understanding and controlling the preparation protocols to improve the performance of the final catalysts. Many investigators have obtained information about, and improved different aspects of, the preparation process using a wide variety of techniques to determine the average changes taking place dur-

* Corresponding author.
E-mail address: crozier@asu.edu (P.A. Crozier).
[1] Present address: ATTD, Intel Corp., Chandler, AZ 85226, United States.

0021-9517/$ – see front matter
doi:10.1016/j.jcat.2008.12.001

ing catalyst preparation. Investigations include studies on diffusion of salt solutions into support extrudates [12], precursor–support interactions in solution [13–15] as well as drying and calcination steps [16,17].

Most methods for characterizing preparation intermediates and the final catalyst provide averaged information on the entire ensemble of particles present in a catalyst. The acquired information is vital in identifying useful catalyst formulations but it cannot provide useful information about nanometer scale variations, which are essential to understand the formation processes of bimetallic catalysts. However, to develop a fundamental understanding of the nucleation and growth processes of nanoparticles, the evolution of the structure and chemistry in individual nanoparticles must also be explored if a deep understanding of the structure–property relations is to be elucidated. For bimetallic systems, characterizing and understanding the origins of heterogeneity in bimetallic particles can help in understanding both the catalyst properties and the catalyst preparation processes.

In situ environmental transmission electron microscope (ETEM) is a powerful approach for understanding the nanoscale structural and chemical modifications taking place, under near-reactor conditions, in catalytic nanoparticles [18–23]. It can avoid many common disadvantages of the *ex situ* characterization techniques, such as the change of nanostructure and chemistry that may occur when the catalyst is removed from the reactor and exposed to air. (It can also avoid changes in the catalyst that may take place due to exposure to vacuum.) We have previously applied this technique to perform *in situ* studies of the atomic scale dynamic processes during the preparation of Ni/TiO_2 and $Co–Ru/Al_2O_3$ catalysts via the incipient wetness route [24–26]. In the present work, we report new results on fundamental dynamic processes taking place during the preparation of Ni–Cu bimetallic nanoparticles supported on high surface area titania (P-25). The nanoscale processes taking place during catalyst preparation and the resulting dispersions may differ significantly in the $CuNi/TiO_2$ system compared to the previously studied $CoRu/\gamma\text{-}Al_2O_3$ system. For the CoRu system, the phase diagram shows the formation of an intermetallic phase when the Ru atomic concentration reaches 33% [27] whereas Cu and Ni are completely miscible in each other making uniform alloying favorable. The uniformity of the bimetallic particles may also be influenced by the choice of metal precursors. In the CoRu study, we used a nitrate of Co and a chloride of Ru which could lead to substantially different interactions between the two metal precursors and the support during the drying and thermal treatments. In the present study, we chose nitrate salts for both metals to make the interaction between the substrate and the solutions more similar. Moreover, in the previous study, the CoRu particles were supported on a non-reducible $\gamma\text{-}Al_2O_3$ support. In the present work, the metal particles are supported on titania, a reducible oxide. During the reduction in hydrogen, a large number of oxygen vacancies will be introduced onto the surface of the titania which may strongly influence diffusion, nucleation and growth processes [28]. In this study we also probe the compositional variations that are present within individual bimetallic particles in the reducing atmosphere.

The preparation is carried out at relatively low temperatures (300 °C) on precursors prepared with the standard incipient wetness method. We present results on the direct atomic level observations of precursor dispersion, Cu enhanced reducibility and the dynamic nucleation, growth and transformation of the metal containing nanoparticles. We show that these observations can be used to explain the formation of uniform bimetallic particles and nonuniform bimetallic particles with Ni surface enrichment. Some of the earlier results from the CoRu study have been employed to facilitate the interpretation of the Ni–Cu data presented here.

2. Experimental procedures

2.1. Precursor preparation

The bimetallic Ni–Cu catalyst precursors were prepared by an incipient wetness technique [29]. Titanium dioxide powder (Degussa P-25, a mixture of about 75% anatase and 25% rutile) was impregnated with the desired amount of $Ni(NO_3)_2{\cdot}6H_2O$ and $Cu(NO_3)_2{\cdot}6H_2O$ salt solutions to generate the precursors containing 3 wt% Ni and 1 wt% Cu. The metal-loaded powder was aged in ambient conditions for 30 min, and then dried in an oven in presence of air at 120 °C for 16 h. A 1 wt% Cu monometallic catalyst precursor was prepared using the same route as above.

Samples for TEM characterization of the initial distribution and chemistry of the precursors were prepared by dispersing the dried precursor powders on the holey-carbon Cu grid. Samples for *in situ* preparation of Ni–Cu and Cu catalysts were prepared by putting the precursors onto 50-mesh pure Pt (99.997%) grids.

2.2. Z-contrast imaging and nanoprobe analysis of the Ni–Cu precursor

The *ex situ* nanoscale structural and chemical characterizations of the Ni–Cu precursor on the titania support were performed in a JEOL 2010F 200 kV Schottky field emission TEM operating in the scanning transmission electron microscope (STEM) mode. A JEOL high-angle annular dark field detector was used to collect *Z*-contrast images from the sample [30]. Furthermore, the small electron probe (with the size of 0.5–0.7 nm) allows us to perform high spatial resolution electron-energy-loss spectroscopy (EELS) chemical analysis [31] on individual nanoclusters. Gatan DigitalMicrograph 3.7.1™ software was used for acquiring the *Z*-contrast images and electron energy-loss spectra.

2.3. In situ reduction of the Ni–Cu precursor and Cu precursor

In situ preparation of the Ni–Cu nanoparticles was performed in a Tecnai F-20 field emission ETEM operating at 200 kV with a point resolution of 0.24 nm. This instrument has a gas reaction cell (i.e. a microreactor) which allows us to perform atomic level observations of gas-solid reactions on catalysts at pressures up to 8 Torr [19,23–26,32,33]. The *in situ* high-resolution electron microscope (HREM) images were recorded with a Gatan CCD camera using DigitalMicrograph 3.1™ software. The ETEM is also equipped with an annular dark-field detector and can perform *Z*-contrast imaging during *in situ* reduction. *Z*-contrast imaging is ideal for differentiating the heavier Ni(Cu) nanoparticles from the lighter titania support. The ETEM is also equipped with a Gatan Imaging Filter; thus EELS can be employed for *in situ* high spatial resolution nano-chemical analysis.

The reducing gas mixture of 20% H_2 mixed with 80% N_2 was admitted into the reaction cell and the pressure was set to 1.5 Torr before the samples were loaded into the TEM column. The initial distribution and morphology of the Ni–Cu precursors supported on the titania was characterized at room temperature before the reduction process. The sample temperature was then ramped up to 300 °C over a period of 2 min. The first observation was made after about 5 min at 300 °C when thermal drift of the TEM holder became manageable. The *in situ* HREM images were acquired with short exposure times to minimize the impact of thermal drift on the images. The temperature and reducing gas pressure were kept constant for up to 2 h. Precautionary steps, such as blanking the electron beam during the experiments except when recording the data, were used to minimize the electron beam irradiation effects. Furthermore, comparison between the non-irradiated and irradiated areas of the sample demonstrated that the use of relatively low-dose electron irradiation did not cause observable effects on

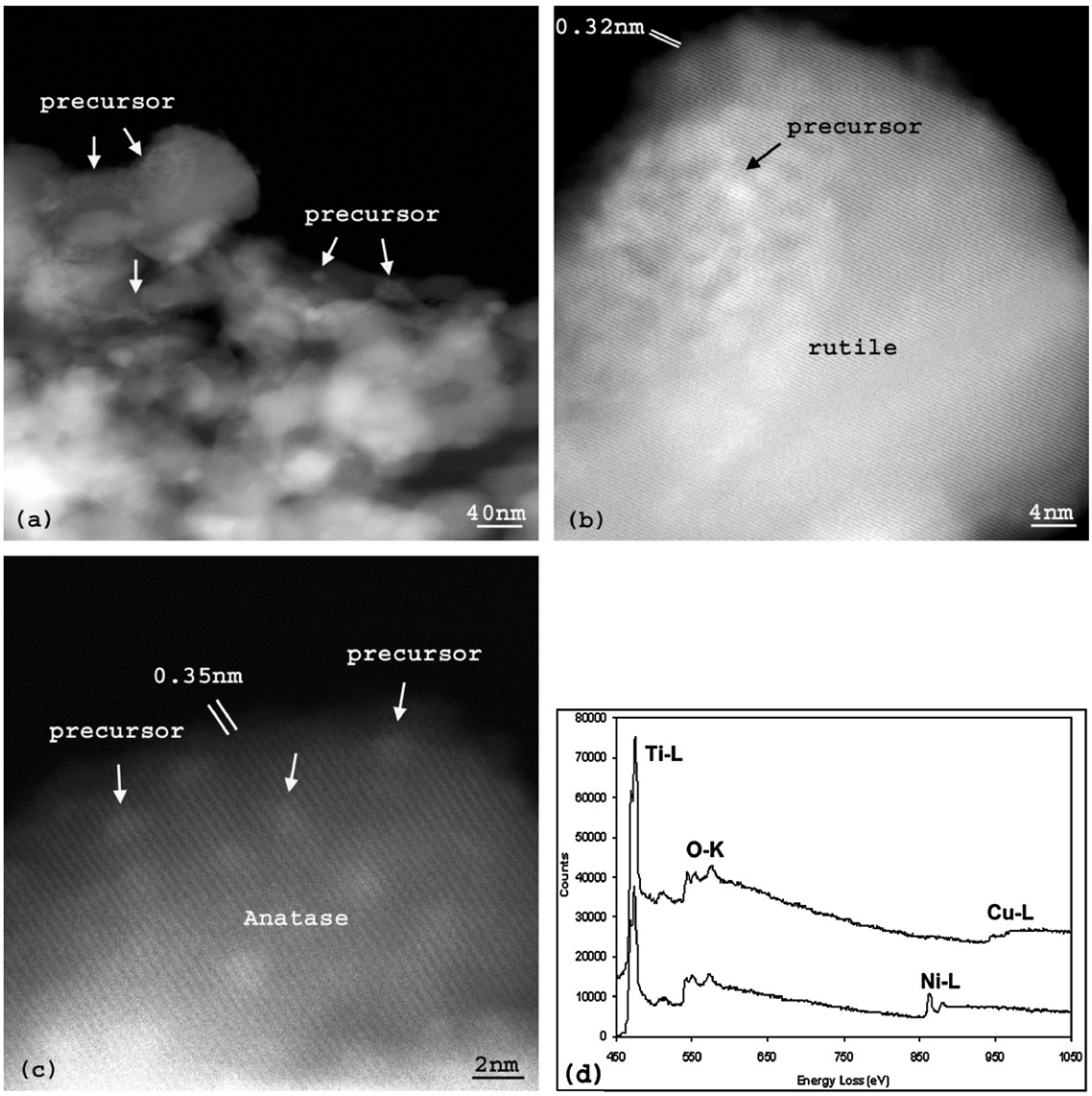

Fig. 1. (a–c) Atomic resolution *Z*-contrast images of Ni and Cu precursors on titania supports and (d) nanoprobe EELS analyses on individual precursor particles.

the *in situ* preparation processes of the catalyst samples. *In situ* reduction of Cu precursor was performed under identical conditions.

An *in situ* EELS line scan technique was used to determine whether uniform alloying or phase segregation occurs within the Ni(Cu) nanoparticles, especially at the surface of the particles. In our experiments, such analyses were performed on over 20 particles after 2 h reduction. A series of 5 to 10 energy-loss spectra were collected by scanning the 0.5 nm electron probe across the selected nanoparticles. A comparatively short acquisition time (i.e. 0.1 s) was used to collect each energy-loss spectrum to minimize the effect of sample drift. The dispersion was 0.5 eV per channel, the energy resolution about 2 eV and the collection semi-angles of about 20 mrad. One big advantage of the *in situ* nanoprobe chemical analyses over the *ex situ* chemical analysis techniques is that the environmentally sensitive catalyst components are not exposed to air, therefore, preserving the nature of the chemistry under real reducing conditions.

In situ nanoprobe EELS analyses were also performed from these particles by placing the electron nanoprobe accurately on the particles. Longer acquisition times (0.5 s) were used to increase the Ni and Cu EELS signals so that quantitatively elemental analysis could be achieved. Furthermore, the relative intensity of peaks at the front of the L_3 and L_2 edges, the so-called white lines, can be used to judge the oxidation states of the Ni and Cu species for individual nanoparticles [31,34]. The L_3 and L_2 white line peaks are, respectively, located at 855 and 872 eV for Ni and at 931 and 951 eV for Cu. The background under the Ni and Cu edges was removed using the standard inverse power-law expression and the small particles size makes plural scattering negligible for the present analysis [31]. However, large thermal drift at 300 °C in H_2 limits the practical acquisition time that can be used for nanospectroscopy yielding spectra from individual nanoparticles that are rather noisy. However, the signal-to-noise was adequate for differentiating gross differences in metal composition and for differentiating between metallic and oxide nanoparticles using the white-line approach. Moreover, with these short exposure times, no electron beam induced changes were observed.

3. Results

3.1. Structural and chemical characterization of Ni–Cu bimetallic precursor

Fig. 1 shows *Z*-contrast images of the initial distribution of Ni and Cu precursors on the titania P-25 support. As indicated by ar-

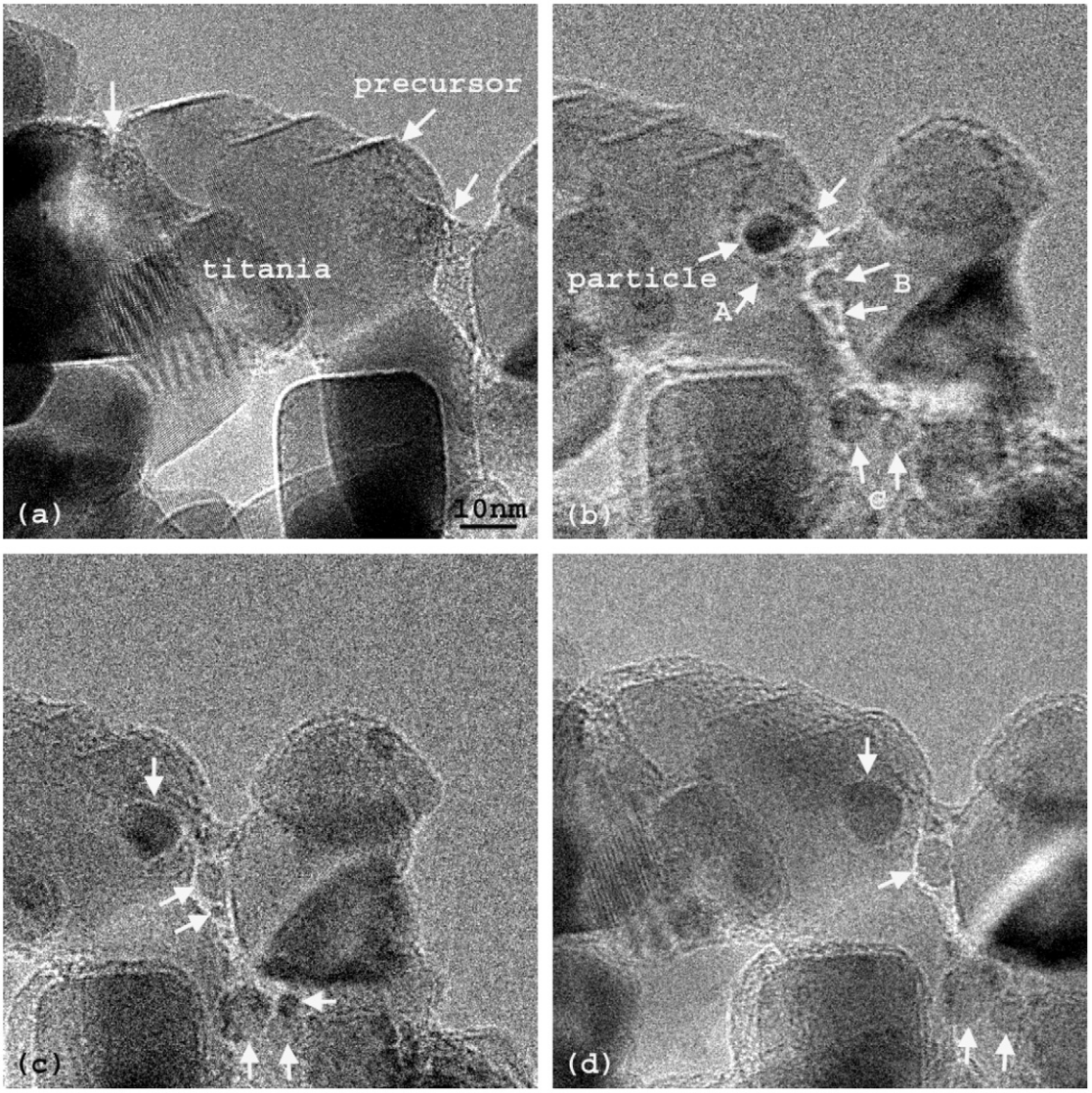

Fig. 2. *In situ* HREM images showing the evolution of Ni–Cu bimetallic particles on TiO_2 support before reduction (a) and after reduced at 300 °C for: (b) 5 min, (c) 15 min, and (d) 60 min under 1.5 Torr of 20% H_2/80% N_2.

rows in the figures, the precursor distributed on the titania support as small particles or patches with sizes around 1–10 nm. Note in Fig. 1c that there is a relatively small *Z*-contrast between the precursor patches and the titania support. This is reasonable because the difference in average atomic number between the precursors and the support is small. The precursor was found to locate on both anatase and rutile particles of the titania support. Fig. 1b shows the precursor particles on the rutile support, where 0.32 nm *d*-spacing corresponds to rutile {101} lattice planes. Whereas in Fig. 1c, the precursor is on the anatase support, where the 0.35 nm *d*-spacing from the support corresponds to anatase {101} lattice planes.

EELS nanoprobe analyses were performed on individual precursor patches and representative results (i.e., spectra 1 and 2) are given in Fig. 1d. In most cases (i.e. 20 out of 23 measurements), either Ni $L_{2,3}$ edges (electron energy loss peak at 850 eV) or Cu $L_{2,3}$ edges (electron energy loss peak at 930 eV) are present in the spectra. We rarely found both metals in the same precursor patch. Both EELS nanoprobe and *Z*-contrast imaging analysis data in Fig. 1 suggest that individual 1–10 nm patches of either Ni-rich or Cu-rich precursor were dispersed uniformly on titania P-25 support.

3.2. *In situ* preparation of the Ni–Cu particles at 300 °C in hydrogen

Fig. 2 is a series of HREM images following the dynamic preparation process of the Ni–Cu bimetallic particles from their precursors. As shown in Figs. 2a and 2b, prior to the reduction, the precursor patches were identified as small black dots with sizes around 1–2 nm on the titania support (indicated by the arrows in Fig. 2a). After 5 min of reduction, small nuclei (indicated by arrows in Fig. 2b) with sizes about 1–3 nm nucleated at certain titania surface sites (i.e., grain boundaries and surface defects). Note in the figure that tiny particles with sizes smaller than 1 nm have nucleated around these larger nuclei. The nucleation and growth events were followed with time at locations labeled by A, B and C in Fig. 2b. As shown in case B, the big nucleus grew and the small particle adjacent to it gradually shrank (shown in Fig. 2c) and finally disappeared (shown in Fig. 2d). Also note in cases A and C, the big nuclei grew while the small particles nearby merged into them and disappeared. The average size of the supported nanoparticles was around 5–10 nm after 2 h reduction and they distributed uniformly on the titania support. Similar particle growth events are also labeled in Figs. 3a–3d where larger particles grew and small particles disappeared or merged into large particles.

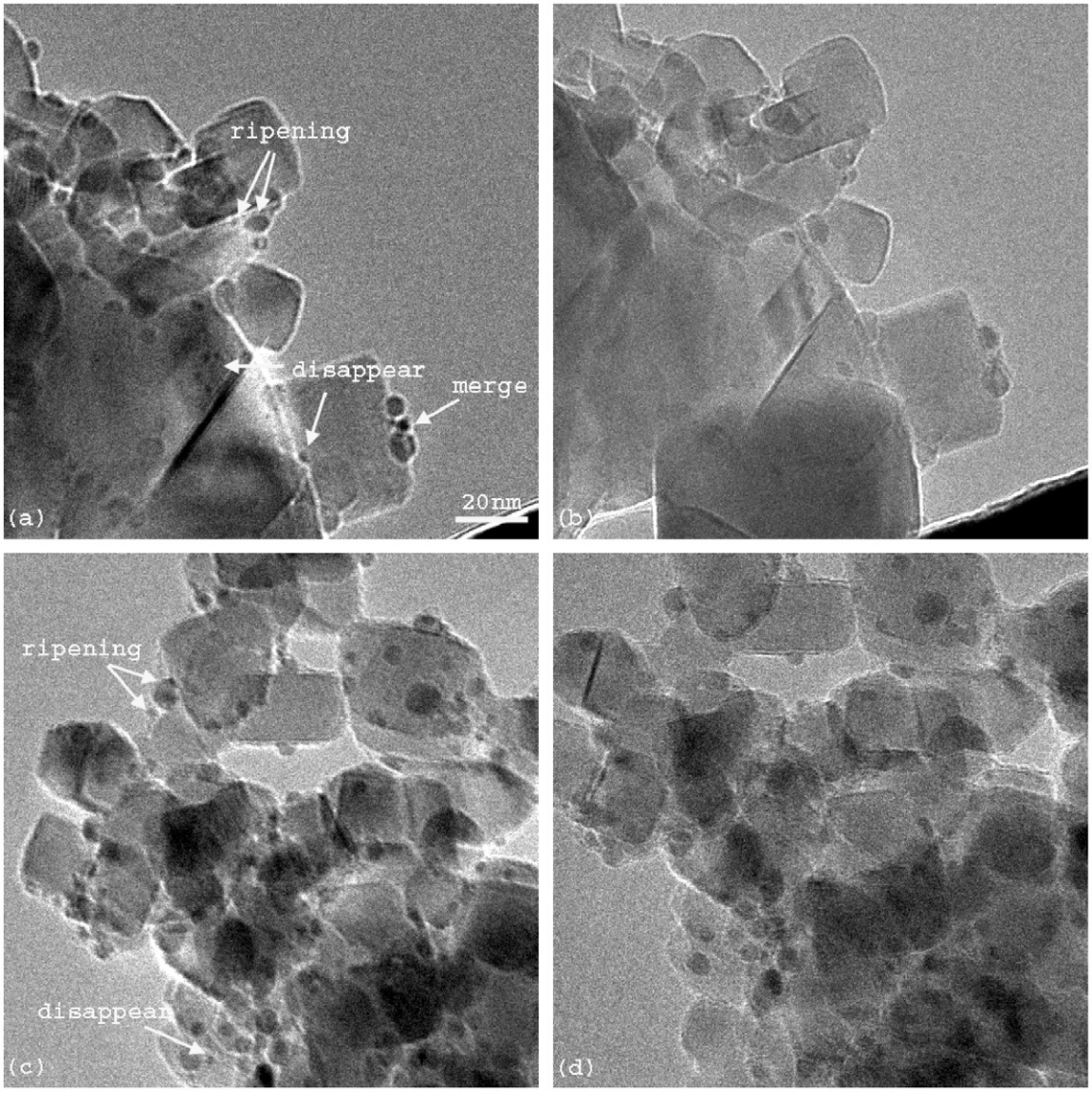

Fig. 3. *In situ* HREM images showing the evolution of Ni–Cu bimetallic particles on TiO_2 support after reduced at 300 °C for: (a) and (c) 20 min, (b) and (d) 120 min under 1.5 Torr of 20% H_2/80% N_2.

Figs. 4a and 4c show *Z*-contrast images of the supported nanoparticles after 2 h reduction. In both figures, higher atomic number metal nanoparticles show with bright contrast on the titania support. *In situ* EELS line scans were performed across individual nanoparticles to explore the variation in the Cu and Ni content within each particle and typical results are shown in Figs. 4b and 4d, respectively. Both figures present five energy-loss spectra acquired from the locations labeled in Figs. 4a and 4c. Fig. 4b shows that Ni and Cu $L_{2,3}$ edges are present at all points in the particle shown in Fig. 4a. There is no white line peak in the Cu signal so it is less prominent than the Ni signal. The Cu/Ni concentration ratio is about 30% and for this nanoparticles we estimate the Cu detection limit for Cu to correspond to a Cu/Ni concentration ratio of about 10%. Furthermore, the relative intensity of the Ni and Cu EELS signals is uniform from the surface (i.e., spectra 1 and 5) and the center (i.e., spectrum 3) of the particle. However, in Fig. 4d, Ni signals are obviously more prominent at the surface of the particle (i.e., spectra 1 and 5). From a total of 22 particles measured, 77% (i.e., 17 out of 22) followed the trend of the Fig. 4b; while 14% (i.e., 3 out of 22) cases take the form of Fig. 4d. In addition, individual particles with separated Ni-rich and Cu-rich grains were occasionally observed (shown in Fig. 6) and will be discussed later.

In situ EELS nanoprobe analyses with improved signal strength were also performed on particles with uniform chemical distribution of Ni and Cu, and representative results are given in Fig. 5. Fig. 5a shows two particles (i.e., particles 1 and 2) of sizes around 5 nm. Spectra 1 and 2 in Fig. 5b acquired from these two particles show the presence of Ni and Cu $L_{2,3}$ edges in both spectra. However, the prominent white lines [34] at the Cu $L_{2,3}$ edges are only present in spectrum 2 (indicated by the arrows) but not in spectrum 1. Quantitative EELS analysis of both spectra [31,34] showed that the ratio of the intensities of L_3 and L_2 white line peaks for Ni (i.e., Ni L_3/L_2) was 1.0 in spectrum 1 and 1.3 (i.e., about 30% increases) in spectrum 2. About 87% of the spectra (i.e., EELS measurements from 20 out of 23 particles) were similar to spectrum 1, where the white lines were not apparent at the Cu $L_{2,3}$ edges and the intensity ratio of Ni L_3/L_2 was in the range of 0.75–1.05.

As presented before, Ni-rich and Cu-rich domains coexisted within a small number of particles. Fig. 6b gives the *in situ* EELS nanoprobe analysis performed on such a particle shown in

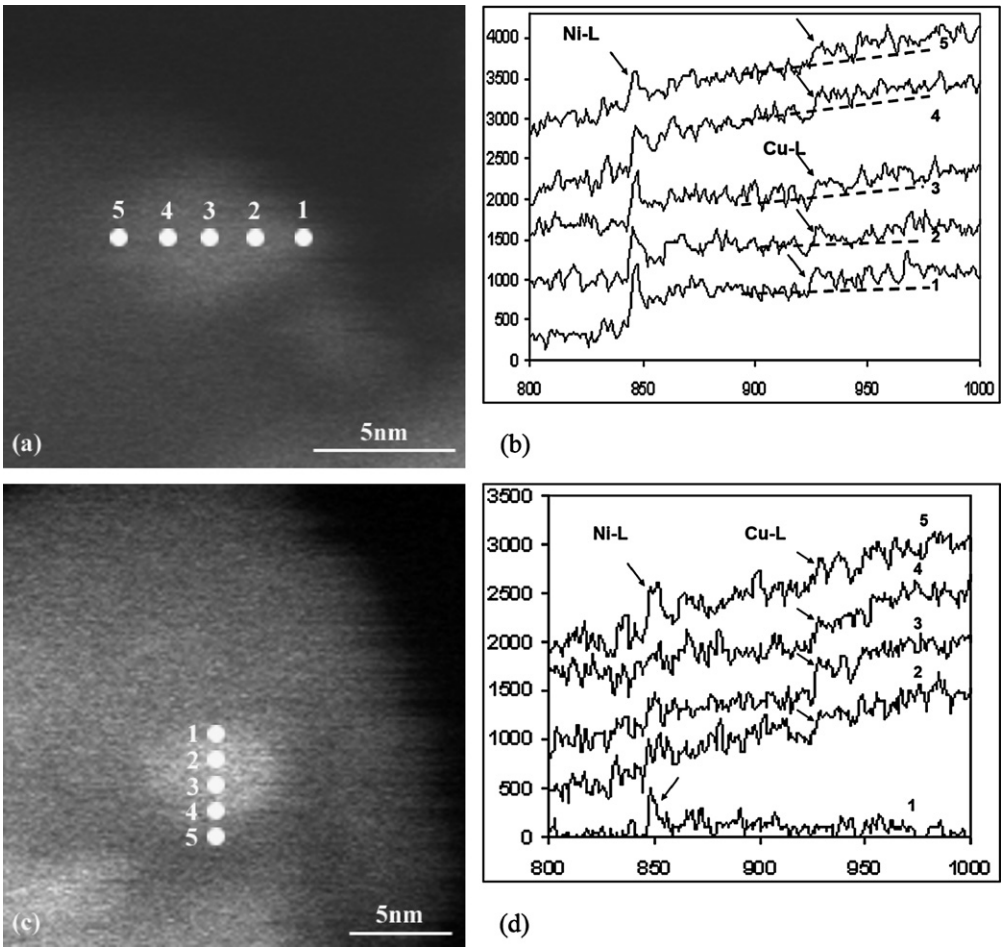

Fig. 4. The *in situ* EELS line scan analysis of the composition distribution across the particles shown in the *in situ* *Z*-contrast images of (a) and (c) are given in (b) and (d), respectively. The experiments were performed at 300 °C under 1.5 Torr of 20% H_2/80% N_2. For clarity, the background under the Cu edge is shown as a dotted line in (b).

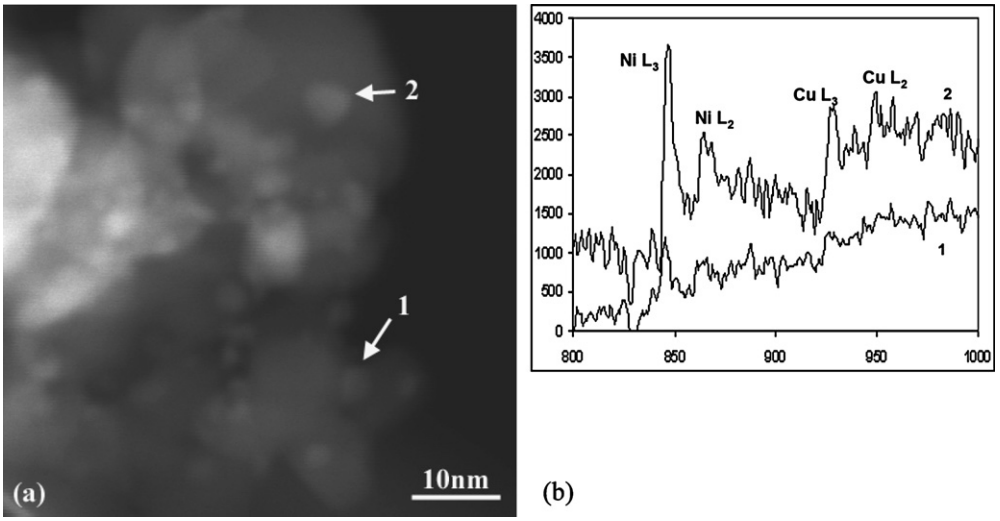

Fig. 5. (a) *In situ* *Z*-contrast image of the nanoparticles and (b) the *in situ* EELS nanoprobe chemical analysis of the particles indicated in (a). The experiments were performed at 300 °C under 1.5 Torr of 20% H_2/80% N_2.

Fig. 6a. It is obvious that spectrum 1, acquired from the upper corner of the particle, shows both Ni and Cu signals, while spectrum 2, acquired from the bottom of the particle, contains only Ni signals. Quantitative EELS analysis showed that the intensity ratios of Ni L_3/L_2 was 1.42 from spectrum 1 and 1.03 from spectrum 2.

3.3. *In situ* preparation of the Cu precursor at 300 °C in hydrogen

Fig. 7a gives the representative *Z*-contrast image of a 15 nm Cu particle on titania after 5 min reduction of the Cu precursor. The chemical state of more than 10 nanoparticles was analyzed by EELS at this early time in the reduction treatment (i.e., between

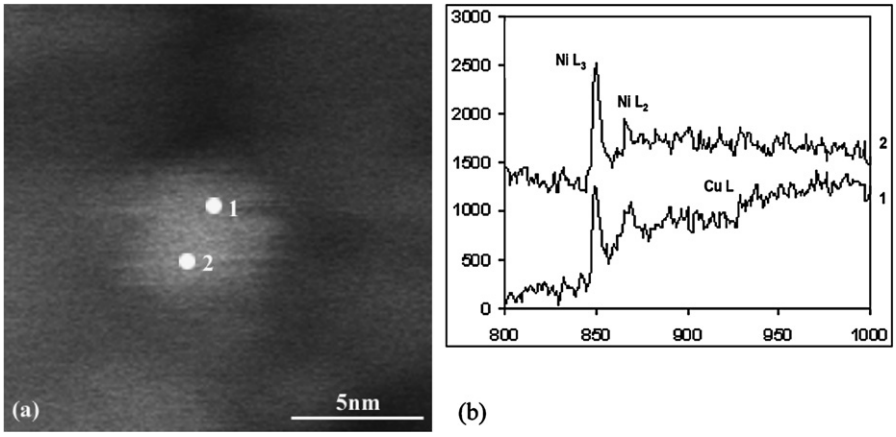

Fig. 6. (a) *In situ* *Z*-contrast image of and (b) the *in situ* EELS precision nanoprobe chemical analysis inside the particle. The experiments were performed at 300 °C under 1.5 Torr of 20% H_2/80% N_2.

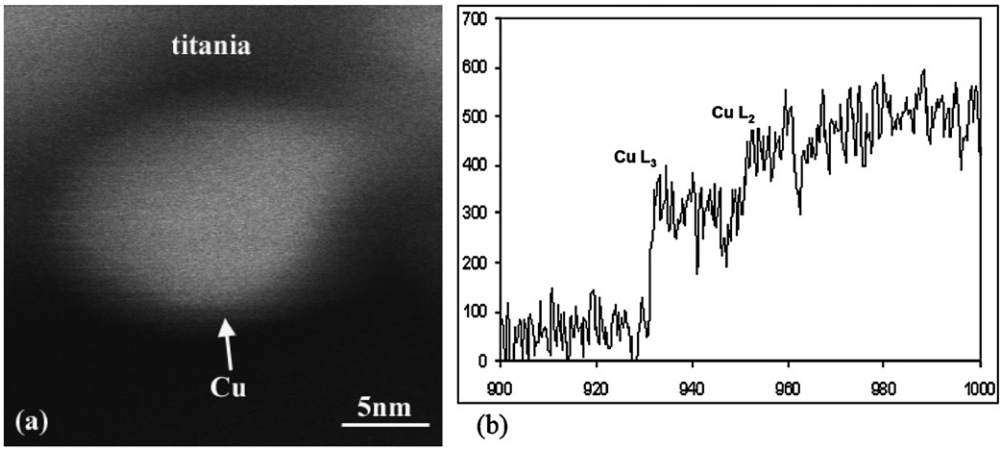

Fig. 7. (a) *In situ* *Z*-contrast image and (b) *in situ* EELS nanoprobe chemical analysis of the nanoparticle reduced at 300 °C for 5 min from Cu precursor on titania under 1.5 Torr of 20% H_2/80% N_2.

5 and 20 min). The representative energy-loss spectrum given in Fig. 7b shows that the prominent white lines (intense peaks at the onset of the ionization edge) at the Cu $L_{2,3}$ edge are absent after only 5 min reduction of the Cu precursor. This showed that, under identical reducing conditions, the pure Cu system reduced much more rapidly compared to that of the NiCu system.

4. Discussions

4.1. Nucleation and growth mechanism of the Ni–Cu bimetallic particles

As presented in Section 3, Ni and Cu precursors mostly separated on the titania support, forming individual Ni-rich and Cu-rich nanopatches with sizes around 1–10 nm. This shows that the efflorescing species is not a homogeneous mixture of the Ni and Cu salts. During drying, it seems likely that one component, perhaps the Ni precursor with the higher salt concentration (3 wt%), will start to effloresce out of solution before the Cu precursor (1 wt%), giving rise to the formation of nickel nitrate nuclei on the titania support. As drying continues, Cu precursor will also start to nucleate out of the solution onto the support. It might be expected that the Cu salt would heterogeneously nucleate on the nickel nitrate crystal. However, our observations showed that this did not happen. Presumably it is more energetically favorable for the Cu phase to nucleate on TiO_2 (defects on TiO_2 may provide preferential nucleation sites) rather than on the Ni salt surface. This drying process generated a heterogeneous distribution of individual Ni and Cu precursor patches on the titania support. The phase separation was on the nanometer scale so it should still be possible to nucleate bimetallic particles at elevated temperature because the diffusion distances are rather short. Individual Ni and Cu precursor patches distributed uniformly on the titania support (i.e., on both anatase and rutile) before reduction. We observed a similar distribution for the pure Cu precursor and this is also consistent with previous work we performed on pure Ni on P25 [24,25].

Our *in situ* experiments were able to record the early stages of the nucleation of small Ni(Cu) nuclei with sizes around 1–2 nm on the support after a fairly short reduction time (i.e., 5 min). It was observed that the location of the nucleus (such as case B in Fig. 2b) was not necessarily the high loading region of the precursor (indicated in Fig. 2a). This indicates that the Ni and Cu precursor species must have diffused quickly to the nucleation sites during the first 5 min of reduction. Some of the nuclei were anchored at certain surface sites of the support such as grain boundaries (shown in Figs. 2 and 3). Grain boundaries in oxides can be favorable nucleation sites for metal particles [35]. These stable nuclei grew at the expense of the surrounding smaller Ni and Cu species. This indicated that during the preparation processes, local Ostwald ripening [36] and/or migration [37] of the smaller Ni and Cu species to the stable nuclei were the major growth mechanisms of the Ni and Cu particles. The main nucleus sometimes merged with nearby smaller nuclei, which indicated that short-range coalescence of the particles can also contribute to the growth of the particles. Long-range migration of particles was not observed

during the *in situ* preparation. This is because the reducing temperature (i.e., 300 °C) is much lower than the Tamman temperatures of Ni and Cu oxide or the metal species (i.e., 405 °C for Cu, 590 °C for Ni, 586 °C for CuO and 841 °C for NiO). Long-range particle migration did not occur during our previous *in situ* preparation of Ni/titania [24,25] and Co–Ru/alumina [26] at temperatures below 400 °C.

4.2. The role of Cu on the reduction of the Ni–Cu precursors

As presented in Section 3.3, the Cu precursor was quickly reduced to Cu metallic particles for the conditions employed in our experiment. After more than 5 min of exposure to the reducing conditions, our *in situ* EELS nanoprobe analyses on many Cu nanoparticles showed that there were no white lines at the Cu $L_{2,3}$ edge onset indicating that the Cu nanoparticles were in the metallic state [31]. All Cu nanoparticles analyzed during the 5 to 20 min reduction period possessed this metallic form. These results are in contrast to the *in situ* preparation experiments we performed on 3 wt% Ni precursor under CO [25]. Even though CO is a stronger reducing agent than H_2 and a higher reducing temperature (i.e., 350 °C) was employed, metallic Ni was observed only after 20 min and many particles needed considerably longer time (up to 2 h) to be fully reduced [26]. *In situ* reduction of 10 wt% Ni precursor under H_2 took 3 to 5 h to fully reduce the Ni containing species to the metallic state [24]. The results on *in situ* preparation of monometallic Cu and Ni nanoparticles suggest that the Cu precursor is much easier to reduce than the Ni precursor. This is consistent with the previously published results on reduction of these two precursors using more traditional conditions and techniques (e.g., [7,38,39]). This shows that the trends observed in the TEM environmental reactor chamber are consistent with higher pressure conditions for these particular systems.

In the bimetallic Ni–Cu system, quantitative EELS nanoprobe analyses were performed on the Ni–Cu particles after 2 h reduction. We observed a correlation between the white line intensities in the Cu and Ni L_{23} edge. The ratio of the intensities of the L_3 to L_2 white lines gives a measure of the oxidation state in 3d transition metals [34]. In Ni, a high L_3/L_2 ratio is associated with oxidized Ni whereas a low value indicates Ni in a more metallic state. In Cu, white lines peaks are associated only with oxide species and are absent when Cu is in the metallic state. Our *in situ* spectra showed that the white line ratio for Ni was about 1.3 when the Cu white lines were present (i.e., Cu is predominantly oxide). When Cu white lines were absent (i.e., predominantly metallic Cu), the Ni white line ratio was about 1.0. The 20–30% decrease in the Ni white line ratio suggests that the Ni is in a more metallic state whenever metallic Cu is present in the bimetallic Ni–Cu nanoparticle.

Further evidence to support this conclusion was apparent from experiments conducted to explore the spatial variation in the chemistry within the small minority of individual nanoparticles which showed compositional heterogeneity. As shown in Fig. 7, the white line ratio of the Ni L_{32} (i.e., 1.06) edge dropped by 27% (from 1.45 to 1.06) when the electron probe moves from the domain containing only Ni to the domain containing both Cu and Ni. This shows that one grain is Ni oxide and the other is Ni(Cu) metal. Furthermore, this indicates that within individual nanoparticles, the oxidation state of Ni is strongly correlated with the oxidation state of Cu. For particles or domains containing both metals, both species are either predominantly in the metallic state or the oxide state.

Our results provide direct evidence that the reducibility of the Ni–Cu precursor is controlled by the reducibility of the Cu species. The presence of metallic Cu enhances or catalyzes the reduction of the Ni precursor. This is consistent with TPR studies on the reduction of Ni–Cu/alumina catalysts, where it was suggested that the addition of Cu to Ni precursors can dramatically lower the reducing temperature of Ni oxides, and might markedly enhance the reducibility of the mixed oxide catalysts [7,39].

4.3. Bimetallic systems: alloying versus segregation

The *in situ* EELS line scan approach described in Section 3.2 is a convenient method for detecting compositional heterogeneity in individual nanoparticles. For most cases, we found that Ni and Cu were uniformly distributed within the particles indicating the formation of homogeneous Ni–Cu solid solution nanoparticles. This is reasonable because of the nucleation and growth events described in Section 4.1. The interpenetrating distributions of Ni and Cu precursor patches on the titania support and the random migration of the Ni and Cu species to specific surface sites almost guarantees the formation of the Ni(Cu) nuclei which will be quickly reduced through the Cu enhanced reduction process. The bimetallic nuclei then grow by ripening and coalescence generating compositionally uniform bimetallic Ni(Cu) particles. In our system, the relatively uniform distribution of the bimetallic Ni(Cu) particles was achieved without introducing the regular calcination step [40], which is normally employed to form the uniform mixed oxide species on the support before the reduction [41].

In the literature on bimetallic Ni–Cu systems, surface segregation of Cu is predominantly reported [10,11]. This is justified on the basis of thermodynamics because the lower heat of sublimation (i.e., lower surface free energy) of Cu compared to Ni leads to Cu occupying the surface sites of the bimetallic particles [11]. However, surface segregation of Ni has been reported in polymer supported NiCu nanoparticles [9]. Moreover, nanoparticles with Ni enriched surfaces have also been generated from Ni and Cu nitrates in ethylene glycol, which acts both as solvent and reducing agent [42]. It was found that the quickly reduced Cu^{2+} ions enhance the reduction of Ni^{2+} [42]. In our data, even though most bimetallic particles were uniformly alloyed, Ni was occasionally found (13% cases) to preferentially segregate to the surface of the bimetallic particles. This can be explained as follows: (1) The Cu precursor reduces more quickly than the Ni precursor, as described in Section 4.2. Therefore, it is easier and quicker to form reduced Cu containing species in the early stage of the reduction process. (2) Cu and CuO have lower Tamman temperatures than Ni and NiO; thus on the titania surface, Cu species diffuse faster than Ni species leading to rapid formation of Cu crystals. (3) The slower diffusion of the Ni species to the Cu-rich nuclei leads to the formation of particles with a Cu-rich core and Ni-rich shell.

This analysis indicates that, the structure of these bimetallic particles is controlled by the kinetics associated with the preparation process and not by thermodynamics. Kinetics dominate the process because we are working at a relatively low temperature. Furthermore, the variation in the final structure of the bimetallic particles is controlled by the interdispersion of Cu and Ni precursor species on the titania. This demonstrates the importance of understanding the kinetics of the preparation process using *in situ* preparation and characterization techniques. The bimetallic nanoparticles with the Ni shell are in a metastable state and will rapidly come into equilibrium at higher temperatures since Ni and Cu are completely miscible. Recent studies by XPS and Auger in Ni–Cu alloys suggest a model that the surface enrichment of Cu can only occur at temperatures above 700 °C where the interfacial energy is high and surface energies is minimized by copper and nickel segregation. For lower Cu loadings and lower temperatures, Ni and Cu form uniform alloyed particles [39]. Our *in situ* experiments, at reducing temperatures of 300 °C, showed the formation of uniform alloy in 85% of the particles and a Ni-rich shell structure in the remaining 15%.

4.4. The nature of diffusion species during reduction

Understanding the nature of the diffusing species can give us a deeper understanding of the fundamental processes taking place during the preparation of bimetallic NiCu particles. Bulk nickel nitrate melts at around 57 °C and our thermal gravimetric analysis (not shown) performed in H_2 suggests that the nitrate is mostly decomposed into oxide by about 200 °C. Copper nitrate melts at a higher temperature of about 170 °C which is still much lower than the reduction temperature we employed. We are not sure how these temperatures will change for the nanoparticles of nitrate on the titania surface. However, it seems likely that the nitrate will decompose at a relatively early stage during the heating leaving either metal or metal oxide species on the support.

By comparing the present observations on pure Cu and CuNi with our previous work on pure Ni and CoRu we can make some deductions about the nature of the diffusing species on the substrate surface. Our previous experiments on the preparation of CoRu particles on alumina system [26] demonstrated that for cobalt nitrate, the transformation from nitrate to oxide also occurred at an early stage. The diffusing species were not metal atoms or clusters because many of the nucleating Co particles formed in the hydrogen atmosphere were oxides. We had similar observations with Ni on titania, the initial particles formed during reduction in hydrogen or vacuum often had a significant oxide component. The observations suggest that for Ni and Co, the predominant diffusing species at 300 °C in hydrogen must be some form of oxide leading to the nucleation of oxide particles. In the pure Cu system, we observe predominantly metallic Cu particles almost immediately after reaching 300 °C in hydrogen. In this case, there are two possibilities for the diffusing surface species; either metallic Cu species are diffusing or oxides species are diffusing. In the latter case, we suppose that reduction to metal will occur more rapidly if the diffusing oxide comes into contact with a metallic Cu particle or a seed crystal.

The presence of some bimetallic particles containing Cu oxide suggests that the main diffusing species may also be Cu oxide. If Cu metal was the diffusing species it seems unlikely that this would be re-oxidized when it combines with NiO species. A more likely outcome of such an encounter is that metallic Cu would facilitate the reduction of the NiO species to metallic Ni. There is a small probability that the Cu metal crystal will not form, leading to the formation of a mixed oxide particles. The resulting mixed oxide particle may have a reducibility which is in between that of CuO and NiO and may not reduce under the conditions employed in our experiment. This interpretation is at least qualitatively consistent with our observations since less than 15% of particles surveyed showed the presence of both oxides. From this analysis we can draw several conclusions. First, starting from metal nitrates of Cu and Ni, the primary diffusing component during reduction in hydrogen at 300 °C is most likely a non-metallic species. Secondly, Cu metal enhances the reduction of Ni oxide species.

5. Conclusions

We have conducted a detailed *in situ* investigation of the initial stages of the formation of the metal and bimetallic nanoparticles during the preparation both Cu on TiO_2 and Ni–Cu on TiO_2 catalysts. The Ni and Cu precursors showed a uniform distribution of nanodomains on the titania support, indicating that there was no preferential distribution of the Ni and Cu precursors on either anatase or rutile during the preparation process. However, in the bimetallic system, the metal containing complexes separated at the nanometer level giving rise to molecularly separate but, on a nanometer scale, intermingled Ni and Cu precursor domains on the support. After initial reduction, many nanoparticles quickly nucleated on the grain boundaries or surface defects of the titania supports. The nanoparticles grew rapidly via the Ostwald ripening or short-range particle–particle coalescence mechanisms.

In situ electron energy-loss nanoanalysis showed that for the Cu precursor alone, metallic particles nucleated and grew rapidly in less than 5 min in a hydrogen atmosphere at 300 °C. For the bimetallic case, both compositionally homogeneous and heterogeneous nanoparticles were formed during reduction. For those particles showing compositional homogeneity, almost 85% of the particles were in the metallic state. The presence of metallic Cu greatly enhanced the reducibility of the Ni species at 300 °C. The diffusing species during the initial reduction process was most likely an oxide leading to the formation of a small minority (15%) of mixed oxide particles. High resolution EELS nanoanalysis also showed that about 15% of all bimetallic particles analyzed were compositionally heterogeneous showing Ni enrichment on the surface. This was a result of the slower diffusion kinetics for the Ni relative to Cu and demonstrated that, at 300 °C in H_2, the surface structure of bimetallic nanoparticles was controlled by kinetics rather than thermodynamics. Our *in situ* atomic scale observations reported in this paper highlight the importance of achieving uniform precursor dispersion on the support in order to develop nanocatalysts with desired structures.

Acknowledgments

This research was conducted using the facilities in the LeRoy Eyring Center for Solid State Science at Arizona State University and was supported by Monsanto Company and the National Science Foundation (NSF-CBET-0553445). The authors thank Mr. K. Weiss for the maintenance of the Tecnai F-20 ETEM. The authors also thank Dr. R. Sharma for the valuable discussions regarding the ETEM.

References

[1] M. Kang, M.W. Song, T.W. Kim, K.L. Kim, Can. J. Chem. Eng. 80 (2002) 63.
[2] T. Huang, S. Jhao, Appl. Catal. A 302 (2006) 325.
[3] R.J. Best, W.W. Russel, J. Am. Chem. Soc. 76 (1954) 838.
[4] M.K. Gharpurey, P.H. Emmett, J. Phys. Chem. 65 (1961) 1182.
[5] Y. Liu, D.Z. Liu, Int. J. Hydrogen Energy 24 (1999) 351.
[6] T. Huang, S. Jhao, Appl. Catal. A 302 (2006) 325.
[7] Y. Li, J. Chen, L. Chang, Y. Qin, J. Catal. 178 (1998) 76.
[8] T. Huang, T. Yu, S. Jhao, Ind. Eng. Chem. Res. 45 (2006) 150.
[9] S. Wu, C. Zhu, W. Huang, Chin. J. Polym. Sci. 14 (1996) 217.
[10] H. Wang, R.T.K. Baker, J. Phys. Chem. B 108 (2004) 20273.
[11] J.H. Sinfelt, Acc. Chem. Res. 10 (1977) 15.
[12] J.A. Bergwerff, T. Visser, B.R.G. Liliveld, B.D. Rossenaar, K.P. de Jong, B.M. Weckhuysen, J. Am. Chem. Soc. 126 (2004) 14548.
[13] M. Schreier, J.R. Regalbuto, J. Catal. 225 (2004) 190.
[14] J.T. Miller, M. Schreier, A.J. Kropf, J.R. Regalbuto, J. Catal. 225 (2004) 203.
[15] L. D'Souza, L. Jiao, J.R. Regalbuto, J.T. Miller, A.J. Kropf, J. Catal. 248 (2007) 165.
[16] Y. Okamoto, Y. Arima, K. Nakai, S. Umeno, N. Katada, H. Yoshida, T. Tanaka, M. Yamada, Y. Akai, K. Segawa, A. Nishijima, H. Matsumoto, M. Niwa, T. Uchijima, Appl. Catal. A 170 (1998) 315.
[17] K.P. De Jong, CatTech 3 (1998) 87.
[18] P.L. Gai, Top. Catal. 8 (1999) 97.
[19] R. Wang, P.A. Crozier, R. Sharma, J.B. Adams, Nano Lett. 8 (2008) 962.
[20] P.L. Hansen, J.B. Wagner, S. Helveg, J.R. Rostrup-Nielsen, B.S. Clausen, H. Topsoe, Science 295 (2002) 2053.
[21] P.A. Crozier, A.K. Datye, Stud. Surf. Sci. Catal. 130 (2000) 3119.
[22] V. Oleshko, P.A. Crozier, R. Cantrell, A. Westwood, J. Electron Microsc. 51 (Supplement) (2002) S27.
[23] R. Sharma, P.A. Crozier, Z.C. Kang, L. Eyring, Philos. Mag. 84 (2004) 2731.
[24] P. Li, J. Liu, N. Nag, P.A. Crozier, J. Chem. Phys. B 109 (2005) 13883.
[25] P. Li, J. Liu, N. Nag, P.A. Crozier, Surf. Sci. 600 (2006) 693.
[26] P. Li, J. Liu, N. Nag, P.A. Crozier, Appl. Catal. A 307 (2006) 212.
[27] T.B. Massalski (Ed.), Binary Alloy Phase Diagrams, William N. Scott Jr., ASM International, Materials Park, OH, 1990.
[28] E. Wahlström, N. Lopez, R. Schaub, P. Thostrup, A. Rønnau, C. Africh, E. Lægsgaard, J.K. Norskov, F. Besenbacher, Phys. Rev. Lett. 90 (2003) 026101.

[29] A.J. van Dillen, R.J.A.M. Terorde, D.J. Lensveld, J.W. Geus, K.P. de Jong, J. Catal. 216 (2003) 257–264.
[30] M.M.J. Treacy, S.B. Rice, J. Microsc. 156 (1989) 211.
[31] R.F. Egerton, Electron Energy-Loss Spectroscopy in the Electron Microscope, Plenum Press, New York, NY, 1986, pp. 255–262.
[32] R.-J. Liu, P.A. Crozier, C.M. Smith, D.A. Hucul, J. Blackson, G. Salaita, Appl. Catal. A 282 (2005) 111.
[33] P.A. Crozier, R. Wang, R. Sharma, Ultramicroscopy 108 (2008) 1432.
[34] D.H. Pearson, C.C. Ahn, B. Fultz, Phys. Rev. B 47 (1993) 8471.
[35] T. Akita, P. Lu, S. Ichikawa, K. Tanaka, M. Haruta, Surf. Interface Anal. 31 (2001) 73.
[36] G.B. Raupp, S.A. Stevenson, J.A. Dumesic, S.J. Tauster, R.T.K. Baker, in: S.A. Stevenson, J.A. Dumesic, R.T.K. Baker, E. Ruckenstein (Eds.), Metal–Support Interactions in Catalysis, Sintering, and Redispersion, Van Nostrand Reinhold Company Inc, New York, 1987.
[37] C.H. Bartholomew, Appl. Catal. A 212 (2001) 17.
[38] R. Naghash, S. Xu, T.H. Etsell, Chem. Mater. 17 (2005) 815.
[39] R. Naghash, T.H. Etsell, S. Xu, Chem. Mater. 18 (2006) 2480.
[40] A.R. Belambe, R. Oukaci, J.G.J. Goodwin, J. Catal. 166 (1997) 8.
[41] E. Iglesia, S.L. Soled, R.A. Fiato, G.H. Via, J. Catal. 143 (1993) 345.
[42] F. Bonet, S. Grugeon, L. Dupont, R. Herrera Urbina, C. Guery, J.M. Tarascon, J. Solid State Chem. 172 (2003) 111.